CHEMICAL ENGINEERING TRANSACTIONS
VOL. 82, 2020
A publication of AIDIC
The Italian Association of Chemical Engineering
Online at www.cetjournal.it
Guest Editors: Bruno Fabiano, Valerio Cozzani, Genserik Reniers

ISBN 978-88-95608-80-8; **ISSN** 2283-9216
DOI: 10.3303/CET2082065

Discrete Element Simulations of Nanoparticles Synthesis in Wet-Operating Stirred Media: Effect of the Particle Material

Marco Trofa[a], Marco Vocciante[b,*]

[a]DICMaPI, Dipartimento di Ingegneria Chimica, dei Materiali e della Produzione Industriale, Università di Napoli Federico II, P.za Giorgio Ascarelli 80, 80125, Napoli, Italy.
[b]DCCI, Dipartimento di Chimica e Chimica Industriale, Università degli Studi di Genova, Via Dodecaneso 31, 16146 Genova, Italy.
marco.vocciante@unige.it

An increasing number of applications from every branch of science and engineering are relying on the use of nanomaterials due to their peculiar properties with respect to the bulk counterpart and the potential of their employment, for example in the environmental field. Hence, there is a growing need to develop alternative strategies to produce such materials, providing first-rate performances and a fine control over the product specifications through safer and more sustainable processes.
Here we focus on a low-energy magnetically driven wet milling technique for the synthesis of metal nanoparticles starting from a bulky solid, as a simple, cheap, and sustainable approach providing numerous advantages, including the minimization of nanoparticle air dispersion and greater control over the final product. We exploit discrete element method simulations to investigate the interactions among the grinding beads and the magnetic stirrer, providing information on the frequency and energy of collisions under various operating conditions, in an attempt to highlight the role of source material in the dynamics of the system. The relation of such data with the properties of the produced nanoparticles allows a fine tuning of the process parameters.

1. Introduction

Nanoparticles (NPs) and nanostructured materials are gradually taking on a central role in the current scientific landscape thanks to their particular properties and their versatility in a wide variety of technical applications. Some examples include medical, industrial (Fabiano et al., 2015), and environmental (Reverberi et al., 2016) applications, to name a few.
So far, the most common production strategies rely on bottom-up approaches, in which NPs are obtained by a progressive aggregation around seeds, typically constituted by ions or molecules, making it easier to monitor the size of the final product (Reverberi et al., 2018b). On the other hand, these methods require the use of various chemicals as reagents, complexing agents, and surfactants, which can have toxic effects on people and environment. For this reason, in a constant attempt to develop new approaches and adopt new procedures that generally refer to 'green nanotechnology' (Reverberi et al., 2017), top-down methods – whereby a nanomaterial is formed starting from elements or compounds in macroscopic sizes undergoing physical treatments without any chemical reaction – are attracting increasing interest (Reverberi et al., 2018b). Several disaggregation techniques have been proposed (Ogi et al., 2017), which consider the possible use of grinding media, such as beads, and stabilizing agents to handle the reaggregation tendency of the as-produced nanoparticles (Ullah et al., 2014). However, the lack of control on the size of the formed NPs (broad distribution) is still a drawback of such methods, thus requiring the adoption of specific strategies.
In the present study, we consider a recently developed top-down physical method based on a mechanical refinement in wet-operating stirred media (Reverberi et al., 2018b). Despite its simplicity, this approach is demonstrating to be particularly promising for the results it manages to deliver in terms of product quality (NPs with reduced size distribution), while remaining intrinsically safe (Fabiano et al., 2019), eco-friendly, and economically sustainable: NPs are produced directly as a suspended phase in the process solvent, minimizing their dispersion in the air and the need for stabilizers or separation processes.

Paper Received: 7 January 2020; Revised: 25 March 2020; Accepted: 7 August 2020
Please cite this article as: Trofa M., Vocciante M., 2020, Discrete Element Simulations of Nanoparticles Synthesis in Wet-operating Stirred Media: Effect of the Particle Material, Chemical Engineering Transactions, 82, 385-390 DOI:10.3303/CET2082065

A crucial aspect in this process is the establishment of particular operating conditions allowing a one-pot bead milling process, where NPs are produced directly starting from a bulky solid like metal spheres of millimetric dimension, which is quite uncommon in literature. Moreover, the well-known rule of thumb established for this type of process, stating that the minimum achievable final diameter of particles may reach 1/1000 of the bead diameter in a wet bead milling equipment, seems to be violated by more than two orders of magnitude in this approach. In fact, as proved by Reverberi et al. (2020), the produced nanoparticles can be smaller than 30 nm, a value corresponding to a $1/10^5$ of the source bead diameter. A possible explanation is related to the distribution and interaction between active and dead zones in the operating volume, which however still requires an appropriate investigation to fully understand and exploit the phenomenon.
In this contribution, the aforementioned process, which is still in development (Reverberi et al., 2020), is investigated by numerical simulations with the purpose of highlighting the effect on the process efficiency of the various parameters, i.e., the physico-chemical properties of the materials used and the operating conditions. In particular, the attention is focused on changes in system dynamics when the setup is used to produce NPs from a different source material. In doing so, the limit case in which the grinding medium is replaced by source beads only is also investigated. Given the high variability of the parameters involved in the setup, this is essential for the optimal design of the process and for the prediction of the nanostructural properties of the final product. Due to the system high confinement and particle volume fraction, its dynamics is primarily governed by particle-particle collisions, thus justifying the use of a Discrete Element Method (DEM) to model, with a certain approximation, the movement of the grinding beads and obtain the collision frequency and impact velocities (Vocciante et al., 2019).

2. Materials and methods

2.1 Experimental set-up

The reference experimental setup is considered as follows:

- cylindrical container (hemispherical base, internal diameter of 13 mm, glass);
- cylindrical magnetic bar (hemispherical ends, diameter of 4.6 mm and length of 15 mm, PTFE coating);
- four silver beads (diameter of 3 mm, Ag, 99.9% (American Elements));
- forty beads of Yttria-stabilized zirconia (diameter of 3 mm, ZrO_2 95%, Y_2O_3 5% (MSE Supplies)).

The stirring bar length is chosen so as it assumes a slanted position in the vessel (with 40° inclination from the horizontal and centre on the container axis 3 mm above the centre of the hemispherical base). The silver beads, assumed as metal precursor undergoing disaggregation, and the zirconia ones (chosen as grinding media for their known high surface hardness and anti-scratch properties) formed a packed bed up to 5 mm below the meniscus of the solution. The stirring bar, rotating around the container axis (300-900 rpm), induces collisions among the particles and the consequent abrasion of the silver spheres with the release of nanoparticles as primary phase. The detailed description of the experimental apparatus mentioned above can be found in Reverberi et al. (2020).

2.2 Numerical set-up

Figure 1 schematically represents the computational domain used in our simulations. Here, the triangular meshes representing the container and the stirring bar (dark grey) are only used to check the contacts with the particles. The yellow and blue beads denote the ZrO_2 and Ag particles, respectively. The centre of the container hemispherical base is set as the origin of a Cartesian reference frame, with the z-axis along the axis of the cylindrical section of the container. The bar mesh is set in uniform circular motion around the container axis.
The discrete element method allows to track the particles by explicitly solving their trajectories (Marshall and Li, 2014). This is done by solving the force and torque balance on each particle:

$$m_\mathrm{p}\frac{d\boldsymbol{u}_\mathrm{p}}{dt} = \sum_j \boldsymbol{F}_\mathrm{c} + m_\mathrm{p}\boldsymbol{g}, \quad I_\mathrm{p}\frac{d\boldsymbol{\omega}_\mathrm{p}}{dt} = \sum_j \boldsymbol{T}_\mathrm{c} \tag{2}$$

where $\boldsymbol{u}_\mathrm{p}$, $\boldsymbol{\omega}_\mathrm{p}$, m_p, and I_p are the particle translational velocity, angular velocity, mass, and moment of inertia, $\boldsymbol{F}_\mathrm{c}$ and $\boldsymbol{T}_\mathrm{c}$ are the contact force and torque acting on a given particle due to the other particles or the walls, and $\boldsymbol{g}$ is the gravity force pointing towards the negative z-direction. The contact force and torque are calculated according to the Hertz-Mindlin model (Trofa et al., 2019). The particle position $\boldsymbol{x}_\mathrm{p}$ and angular position $\boldsymbol{\theta}_\mathrm{p}$ are then updated by integrating the following kinematic equations:

$$\frac{d\boldsymbol{x}_\mathrm{p}}{dt} = \boldsymbol{u}_\mathrm{p}, \quad \frac{d\boldsymbol{\theta}_\mathrm{p}}{dt} = \boldsymbol{\omega}_\mathrm{p} \tag{1}$$

As already done in Vocciante et al. (2019), due to the system high volume fraction, the initial random particle positions are obtained by adding the particles in a cylindrical domain with the same diameter of the container and height 30 mm, placed above the stirring bar at z = 10 mm, and letting them settle. The other initial values are set to zero, i.e., $\boldsymbol{u}_{\mathrm{p},0} = \boldsymbol{\theta}_{\mathrm{p},0} = \boldsymbol{\omega}_{\mathrm{p},0} = \mathbf{0}$.

Figure 1: Representation of the simulation domain, magnetic bar, and beads (yellow for ZrO_2 and blue for Ag).

The properties of the materials considered have been taken from the literature (see Fragnière et al. (2018) for zirconia and glass, Smith and Fickett (1995) for silver, and Gondret et al. (2002) for PTFE) and are listed in Table 1, which also shows copper data (Marshall and Li, 2014) to facilitate the comparison with our previous work (Vocciante et al., 2019).

Table 1: Model parameters and material properties

	Zirconia, ZrO_2	Copper, Cu	Silver, Ag	Glass	PTFE
Density [kg/m^3]	6067	8930	10490	2510	2200
Young's Modulus [GPa]	210.0	120.0	82.0	70.0	0.50
Poisson ratio	0.31	0.33	0.37	0.24	0.46
Coefficient of restitution	0.92	0.65	0.80	0.99	0.80
Coefficient of friction	0.15	0.12	0.55	0.27	0.08

The time step is set to 10^{-7} s, a value much smaller than the actual collision time whose scale is given by the Rayleigh and Hertz time, thus ensuring a correct resolution of the impacts and the stability of the numerical simulations (Marshall and Li, 2014). The impacts, detachments, and then collision duration are obtained by identifying the changes in contacts among particles and walls at every time step. The energy of collision is estimated (upper limit) from the relative velocity at the beginning of a contact (Beinert et al., 2015), and is decomposed in normal and tangential direction. The sampling of the contacts is performed at 0.5 s for 0.1 s when the system has reached a pseudo steady state condition, after the initialization transient in which the particles are free falling in the container. The results are averaged over five simulations with different initial random particle distributions to obtain statistical invariance. The open-source software LIGGGHTS® 3.8.0 has been used to implement and execute the code (more details can be found in Kloss et al. (2012)).

3. Results

The total translational and rotational kinetic energy ($ke = 0.5 \sum m_{\mathrm{p}} u_{\mathrm{p}}^2$ and $ke_{\mathrm{rot}} = 0.5 \sum I_{\mathrm{p}} \omega_{\mathrm{p}}^2$), reported in Figure 2 for the ZrO_2-Ag system and the three stirring velocities considered, confirms the achievement of a dynamic equilibrium condition with an almost constant mean value proportional to the rotation velocity. Such regime is reached after an initial overshoot due to the initialization procedure in which the particles are free falling in the container. The trends are similar to those reported in Vocciante et al. (2019) for the ZrO_2-Cu system and also to the ones for the system with all Ag particles (not shown), which only presents slightly higher values due to the increased mean particle density and friction coefficient (Table 1). The pseudo steady-state condition is confirmed by the collision frequencies among the particles, showing a similar number of impacts in different sampling windows, which is inversely proportional to the rotation velocity. Indeed, around 10900, 5900, and 3200 collisions are detected in the time window 0.5–0.6 s for the cases 300, 600, and 900 rpm, respectively.

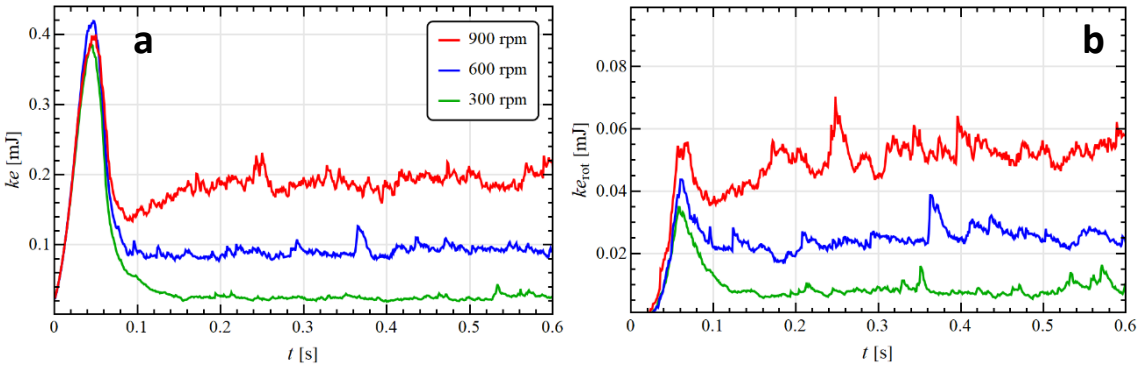

Figure 2: Total translational (a) and rotational (b) kinetic energy for the ZrO_2-Ag system at different stirring velocities.

Figure 3 shows on the left column the duration of the collisions and on the right column the normal component of the relative velocity at the beginning of contacts ($u_{r,n} = (\boldsymbol{u}_{p,i} - \boldsymbol{u}_{p,j}) \cdot \boldsymbol{n}$, with $\boldsymbol{n}$ the normal vector to the contact plane), for the collisions involving at least one source particle and different stirring velocities. Here, the results for the ZrO_2-Cu system (panel a and b), adapted from Vocciante et al. (2019), are also reported for reference.

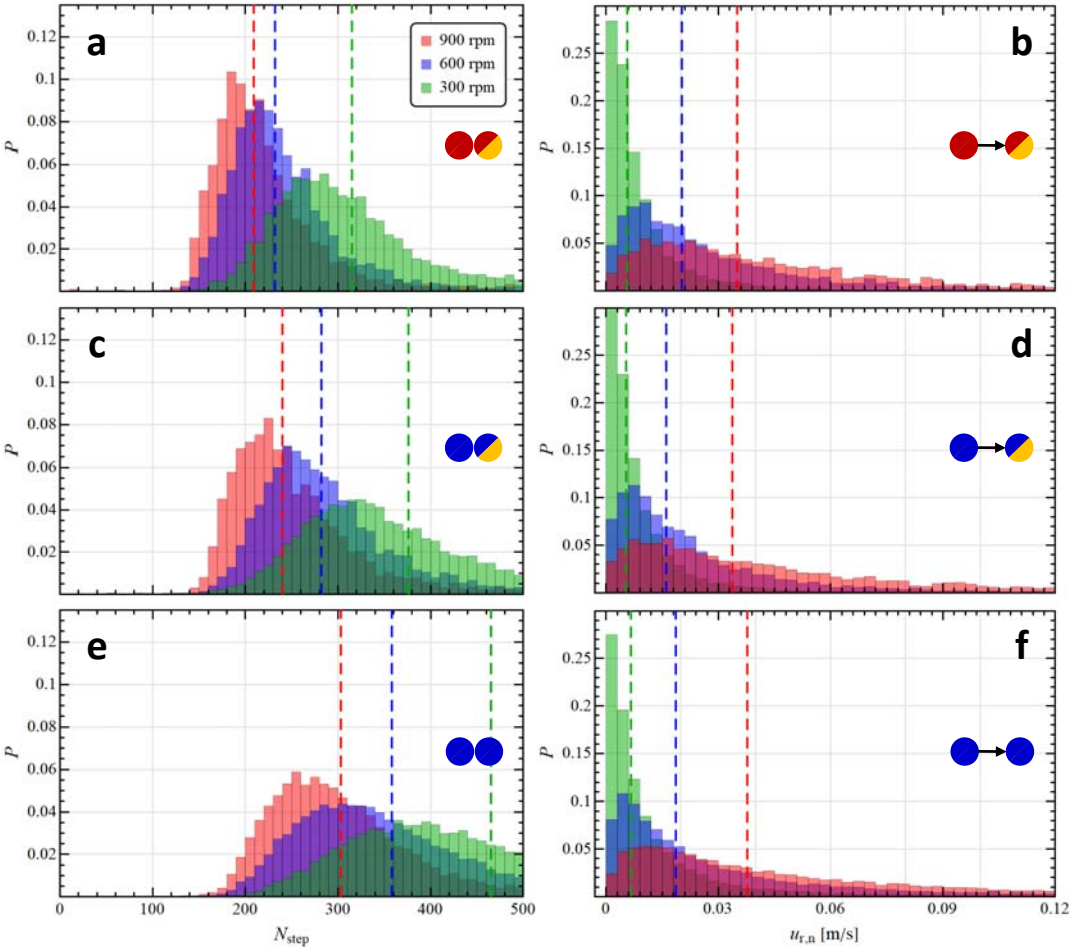

Figure 3: Probability distribution of the contact time (left) and normal impact velocity (right) for the collisions involving at least one source particle at different stirring velocities: (a-b) ZrO_2-Cu system (adapted from Vocciante et al. (2019)), (c-d) ZrO_2-Ag system, (e-f) Ag-Ag system.

In order to ease the comparison among samples of different size, e.g., due to different stirring velocities or type of particles involved, the histograms in Figure 3 are presented in terms of probability, i.e., the fraction of data corresponding to each bin. The distributions are all unimodal and their medians are indicated by dashed lines. In all the investigated cases the collisions last more than 100 time steps (see left panels), equivalent to 10 μs, thus confirming a correct resolution of the contact itself.
An increase in the rotation velocity of the stirring bar determines a shift to lower contact times and a narrowing of the distribution. Such behaviour is related to an increase in the velocity particles are moving and colliding with (right column). The change in source particle material from Cu to Ag determines an increase in the collision time (panel c) but seems not to affect the normal relative velocity at the beginning of contacts (panel d). The first can be primarily related to the reduction in elasticity modulus from Cu to Ag and further corroborated by the increase in density. The second result indicates that Ag and Cu behave in the same way in the particle bed and their collisions with zirconia are slightly slower than the ones between ZrO_2 particles (compare Figure 3b in Vocciante et al. (2019)), probably because of the metals higher density/inertia. The same trend is confirmed for the system with only Ag particles, where the collision time is further increased while the normal impact velocity practically stays the same. This means that the overall particles bed is slowed down as respect to the case with ZrO_2.

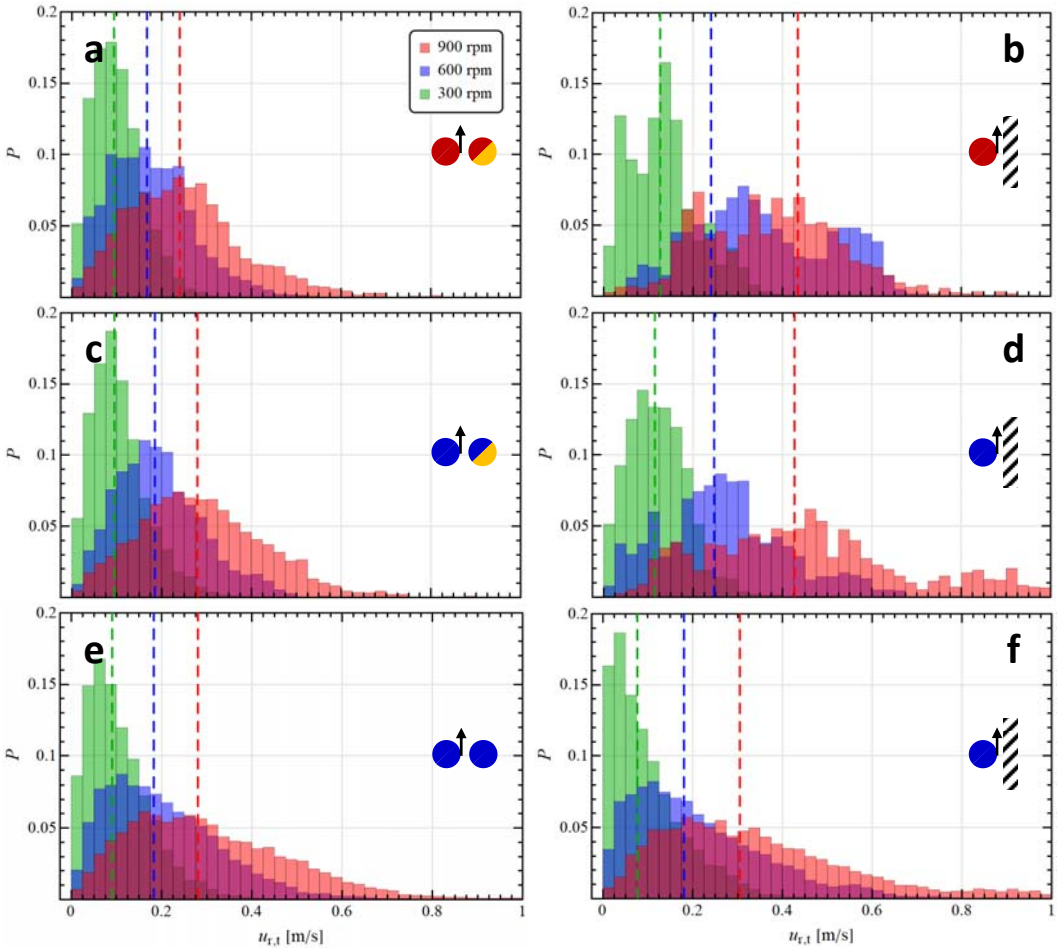

Figure 4: Probability distribution of the tangential impact velocity among the particles (left) and with the container wall (right) for the collisions involving at least one primary particle at different stirring velocities: (a-b) ZrO_2-Cu system (adapted from Vocciante et al. (2019)), (c-d) ZrO_2-Ag system, (e-f) Ag-Ag system.

The tangential component of the impact velocity ($u_{r,t} = \left\|(\boldsymbol{I} - \boldsymbol{nn}) \cdot (\boldsymbol{u}_{p,i} - \boldsymbol{u}_{p,j}) - r_p(\boldsymbol{\omega}_{p,i} + \boldsymbol{\omega}_{p,j}) \times \boldsymbol{n}\right\|$, with $\boldsymbol{I}$ the identity tensor and r_p the particle radius) among particles (left column) and the container wall (right column) is reported in Figure 4. Since the bead mill system is mainly governed by shear imposed by the rotation of the stirring bar, the impact velocity has a tangential component much higher than the normal one, the first being of the order of the bar tip speed (about 0.6 m/s for 900 rpm).

The trends are the same seen before for the normal impact velocity, with a negligible effect of the change in source particle material from Cu to Ag. As regarding the impacts with the container wall, which are in number around 40% than the interparticle collisions, the fewer data for the ZrO_2-Cu and ZrO_2-Ag system (panels b and d) are more scattered but confirm the fact that in these cases the whole particle bed is moving faster as respect to the Ag-Ag system, where the tangential impacts among particles and wall are comparable.

4. Conclusions

In this work, we use discrete element simulations to analyse the effect of source particle material on the impact velocities in a ball mill for three different rotor speed. To guarantee statistical invariance the average values from several simulations with different initial random particle distributions are considered.
All the cases analysed show a stable dynamics, with a nearly uniform (in time) impact velocity and frequency, the latter being inversely proportional to the stirring bar velocity. Ag and Cu particles are proved to be equally suitable to produce NPs in this experimental setup as the bed dynamics and the impact velocities are comparable. In particular, the tangential impact velocity, being around one order of magnitude higher than the normal one, is confirmed to be the main actor in the process of surface abrasion. Remarkably, also a system composed of all source metal particles shows a similar behaviour in terms of interparticle collisions, some differences being visible only for the impacts with the container wall as a consequence of an increased inertia of the bed. This result encourages further experimental testing on the discussed configuration for the development of safer and eco-friendly NPs synthesis processes relying on autogenous systems.

References

Beinert S., Fragnière G., Schilde C., Kwade A., 2015, Analysis and modelling of bead contacts in wet-operating stirred media and planetary ball mills with CFD–DEM simulations, Chemical Engineering Science, 134, 648–662.

Fabiano B., Pistritto F., Reverberi A., Palazzi E., 2015, Ethylene-air mixtures under flowing conditions: a model-based approach to explosion conditions, Clean Technologies and Environmental Policy, 17, 1261–1270.

Fabiano B., Reverberi A.P., Varbanov P.S., 2019, Safety opportunities for the synthesis of metal nanoparticles and short-cut approach to workplace risk evaluation, Journal of Cleaner Production, 209, 297–308.

Fragnière G., Beinert S., Overbeck A., Kampen I., Schilde C., Kwade A., 2018, Predicting effects of operating condition variations on breakage rates in stirred media mills, Chemical Engineering Research and Design, 138, 433–443.

Gondret P., Lance M., Petit L., 2002, Bouncing motion of spherical particles in fluids, Physics of fluids, 14(2), 643–652.

Kloss C., Goniva C., Hager A., Amberger S., Pirker S., 2012, Models, algorithms and validation for opensource DEM and CFD–DEM, Progress in Computational Fluid Dynamics, an International Journal, 12(2-3), 140–152.

Marshall J.S., Li S., 2014, Adhesive particle flow, Cambridge University Press, New York, USA.

Ogi T., Zulhijah R., Iwaki T., Okuyama K., 2017, Recent progress in nanoparticle dispersion using bead mill, KONA Powder and Particle Journal, 34, 3–23.

Reverberi A.P., Salerno M., Lauciello S., Fabiano B., 2016, Synthesis of copper nanoparticles in ethylene glycol by chemical reduction with vanadium (+2) salts, Materials, 9(10), 809.

Reverberi A.P., Vocciante M., Lunghi E., Pietrelli L., Fabiano B., 2017, New Trends in the Synthesis of Nanoparticles by Green Methods, Chemical Engineering Transactions, 61, 667–672.

Reverberi A.P., Varbanov P.S., Vocciante M., Fabiano B., 2018 a, Bismuth oxide-related photocatalysts in green nanotechnology: A critical analysis, Frontiers of Chemical Science and Engineering, 12(4), 878–892.

Reverberi A.P., Varbanov P.S., Lauciello S., Salerno M., Fabiano B., 2018 b, An eco-friendly process for zerovalent bismuth nanoparticles synthesis, Journal of Cleaner Production, 198, 37–45.

Reverberi A.P., Vocciante M., Salerno M., Ferretti M., Fabiano B., 2020, Green synthesis of silver nanoparticles by low-energy wet bead milling of metal spheres, Materials, 13(1), 63.

Smith D.R.; Fickett F.R., 1995, Low-temperature properties of silver, Journal of Research of the National Institute of Standards and Technology, 100(2), 119–171.

Trofa M., D'Avino G., Sicignano L., Tomaiuolo G., Greco F., Maffettone P.L., Guido S., 2019, CFD-DEM simulations of particulate fouling in microchannels, Chemical Engineering Journal, 358, 91–100.

Ullah M., Ali M.E., Hamid S.B.A., 2014, Surfactant-assisted ball milling: A novel route to novel materials with controlled nanostructure - A review, Review on Advanced Materials Science, 37, 1–14.

Vocciante M., Trofa M., D'Avino G., Reverberi A.P., 2019, Nanoparticles Synthesis in Wet-operating Stirred Media: Preliminary Investigation with DEM Simulations, Chemical Engineering Transactions, 74, 31–36.